Extreme Mechanics Letters 35 (2020) 100621

Contents lists available at ScienceDirect

Extreme Mechanics Letters

journal homepage: www.elsevier.com/locate/eml

Combination of stiffness, strength, and toughness in 3D printed interlocking nacre-like composites

Fan Liu [a], Tiantian Li [b], Zian Jia [a], Lifeng Wang [a,*]

[a] Department of Mechanical Engineering, Stony Brook University, Stony Brook, NY 11794, USA
[b] Engineering Department, Cambridge University, Trumpington Street, Cambridge, CB2 1PZ, UK

ARTICLE INFO

Article history:
Received 29 October 2019
Received in revised form 6 December 2019
Accepted 9 December 2019
Available online 16 December 2019

Keywords:
Bio-inspired materials
Nacre
Interlocking
3D printing
Toughening mechanism

ABSTRACT

Constituted by mineral tablets and organic interlayers, nacre is known for its attractive combination of stiffness, strength, and toughness. The impressive mechanical property of nacre can be attributed to the 'brick-and-mortar' structure which is usually defined with two geometric parameters: tablet aspect ratio and volume fraction of the stiff phase. Inspired by the interlocking tablets found in red Abalone and *Hyriopsis cumingii*, we study the effect of interlock by introducing a third parameter: tablet waviness angle. Tension tests and single edge notched bend fracture tests are performed on the specimens of interlocking and non-interlocking nacre-like composites that are fabricated using a high-resolution multi-material 3D printer. Stress distribution, deformation pattern and parameter analysis reveal the mechanical behavior of interlocking and non-interlocking nacre-like composites and how these three parameters affect the performance. Two failure patterns (soft phase failure and tablet break) and three toughening mechanisms (uncracked-ligament bridging, constrained microcracking, and crack deflection/twist) are found in three-point bending fracture tests, which uncovers the key to high toughness. Interlocking nacre-like composites clearly show enhanced tensile and fracture performance with an unusual combination of stiffness, strength, and toughness.

1. Introduction

To adapt to the highly competitive environment, nature has evolved diverse biomaterials with incredible mechanical performance [1–4]. The biomaterials are usually made of small repeated building blocks and their unique properties originated from the finely designed structures of these building blocks. To understand the mechanics of biomaterials and in turn to design bio-inspired materials, the structure of the building blocks needs more in-depth investigations. Nacre is known for its attractive combination of stiffness, strength, and toughness. The impressive mechanical property of nacre can be attributed to its building block: the 'brick-and-mortar' structure. Researchers have made a lot of efforts to understand the detailed structures of the building block of nacre and its effects on the mechanical properties. The 'brick-and-mortar' structure comprises of about 95% Aragonite (stiff phase tablet with Young's modulus of 50–100 GPa) and few percent of organic macromolecules (soft phase interlayer with Young's modulus of 50–100 MPa) [5]. In addition to the simple 'brick-and-mortar' structure, more detailed structures are found that contribute to the toughness of the nacre. For example, mineral bridges are found in the organic matrix layers [6], nanoscale mineral islands are found on the top and bottom surface of tablets [7], tablet waviness, and tablet interlocks are observed in some species of nacre. Moreover, unique nanoparticle–biopolymer architectures are observed in nacre's aragonite platelets that are previously considered brittle, enabling tunable crack propagation inside the aragonite platelets and greatly enhancing the toughness and strength [8–10]. The basic 'brick-and-mortar' structure and detailed sub-level structures mentioned above all affect the interactions of hard and soft materials, which are the keys to the exceptional mechanical properties of nacre [2,11–13].

One important goal of studying biomaterials is to mimic the exquisite structure of biomaterials for developing bio-inspired artificial materials with advanced mechanical performances. Researchers have tried many ways to fabricate artificial nacre. Layer-by-layer assembly technique, cross-linking strategy, and laser engraving technique are used to fabricate nacre-like composites with stiff tablets and soft interlayers [14–16]. Some researchers fabricated nacre-like composites with enhanced mechanical property by modifying the surface of tablets or introducing interlocking tablets [17,18]. Interestingly, mother nature constructs nacre from bottom up by using nanoparticles during biomineralization process [19], which is very similar to the widely

* Corresponding author.
E-mail address: Lifeng.wang@stonybrook.edu (L. Wang).

https://doi.org/10.1016/j.eml.2019.100621
2352-4316/

used tools in fabricating nacre-like composites and other bio-inspired materials — 3D printing, despite that current 3D printing techniques still have large room for improvement to compare with self-assembly method and biomineralization process [20]. Compared to traditional fabrication techniques, 3D printing can create bio-inspired materials with accurate-and-precise structure details. Due to that, systematical investigation of effects of structure details on the mechanical performance become possible. Many researchers have studied the effects of structure details on the mechanical performance of 3D printed bio-inspired materials [21–27]. Nacre-like composites have been fabricated in the studies done by Viacheslav et al. [28], they have showed different failure mode of nacre-like composites under loading with different inclination angles. In the work of Askarinejad et al. [29], they have demonstrated that increasing the waviness of tablets can improve the stiffness, strength, and toughness of the nacre-like composites. Lee et al. [30] have designed nacre-like composites with topologically interlocked blocks and investigated the effect of topological interlock on mechanical performance of nacre-like composites. Impact behavior of nacre-like composites and effects of structure details on impact behavior have also been studied [31–33]. Although many researchers have worked on the nacre-like composites and some of them studied the effect of interlock on the mechanical property, the toughening mechanisms with a focus on the failure modes transform still needs further discussion, which is the key to the design of interlocking nacre-like composites.

In this study, a 3D printing technique is employed to fabricate tensile and single edge notched bend (SENB) specimens of interlocking and non-interlocking nacre-like composites. To systematically investigate the effect of the design parameters, i.e., tablet waviness angle θ, tablet aspect ratio η, and volume fraction of stiff phase ρ, groups of specimens with different controlled parameters are fabricated, tested and compared. We further study the deformation and stress distribution of these specimens using finite element simulation. The results of deformation, failure pattern, and toughening mechanisms investigated through this study reveal the effects of geometric parameters on the mechanical performance of nacre-like structures.

2. Materials and methods

2.1. Characterization of nacre-like composites

In this study, the model system of nacre-like composites consists of two phases: the soft phase (light gray) and the stiff phase (dark gray) (Fig. 1). Mimicking the nacre with different tablet waviness angles in nature (Fig. 1(a–c)), two types of nacre-like composites are considered with different tablet waviness angles: interlocking nacre-like composites — tablet waviness angle $\theta < 0°$; non-interlocking nacre-like composites: — tablet waviness angle $\theta \geq 0°$. Three basic parameters, namely, the volume fraction of the stiff phase, ρ, the tablet aspect ratio, η, and the tablet waviness angle θ fully define the interlocking and non-interlocking nacre-like composites. The tablet aspect ratio η is defined as $\eta = \frac{L-t}{w}$. Other geometric parameters can be calculated from these three parameters.

2.2. Sample fabrication

All specimens in this study were fabricated using an Objet Connex260 3D printer (Stratasys, Ltd) which has a minimum resolution of 0.016 mm and allows printing two materials simultaneously. VeroWhite is used as the stiff phase material and TangoPlus is used as the soft phase material. The specimens for tensile tests consist of 8×4, 4×4 and 4×4 unit cells, when $\eta = 2$, 5, and 10 respectively, and the dimension is $a \times 20$ mm $\times 5$ mm (Fig. 1(e)). The specimens for 3-point bending tests consist of $N \times 10$ unit cells and the dimension is 112.5 mm $\times$ 25 mm $\times$7.5 mm (Fig. 1(d)). Note that the parameters a and N vary with the aspect ratio and volume fraction. In order to minimize the influence of printing direction on mechanical properties, all specimens are printed along the same direction on the panel.

2.3. Mechanical tests

To capture the mechanical response of the nacre-like composites, uniaxial tensile tests and 3-point bending tests are performed using an MTS mechanical tester (C43) with 1 kN and 10 kN load cells (Fig. 1(d) and (e)). Both tensile and three-point bending tests are conducted in a quasi-static regime. The strain rate for the tensile tests is 0.001 s^{-1} and the displacement rate for the 3-point bending tests is 0.5 mm/min. The mechanical tests are performed on the samples 24 h after printing. Load–displacement curves from tensile tests are transferred to nominal stress–strain curves while Young's modulus and yield stress are calculated based on these curves. The toughness is measured from the load–displacement curves of 3-point bending tests. The toughness here is defined as the area under the force–displacement curve which represents the energy absorbed and dissipated before catastrophic failure. This definition is wildly used in rigid biological composites [36]. Images of the specimens during the loading procedures are captured at a rate of 1 FPS. Strain fields are calculated with a digital image correlation (DIC) method (VIC-2D, Correlated Solution Inc.).

2.4. Finite element analysis

Numerical simulations are conducted using the commercial finite element (FE) package ABAQUS/Standard to capture the mechanical response of the tensile specimens. The stiff phase of the structure is generated by plane strain elements CEP4 with an elastic–plastic model where Young's Modulus is 1.93 GPa, the Poisson's ratio is 0.33, and the yield stress is 53.2 MPa. The soft phase of the structure is generated by plane strain elements CEP4 with one layer of cohesive element COH2D4 inserted in the central line of the soft phase. For the soft phase with CEP4 elements, a linear elastic model is used with Young's modulus of 30 MPa and the Poisson's ratio of 0.4. For the soft phase with cohesive elements, the traction-separation model is used to define the damage property. Maximum nominal stress criterion is used to define the damage initiation with maximum normal stress equal to 4 MPa and maximum shear stress equal to 2.5 MPa. Mixed-mode damage evolution is defined with Power Law form. Normal mode fracture energy is 0.8 kJ/m^2, and shear mode fracture energy is 1.8 kJ/m^2. Geometric and material nonlinearities are considered to enable large deformation. In addition, finite element models used in the structure is verified by a mesh sensitivity test.

3. Results and discussion

3.1. Mechanical response under tension

We start by investigating the tensile response of nacre-like composites experimentally and numerically and study how the geometric parameters including tablet waviness angle θ, tablet aspect ratio η, and volume fraction of the stiff phase ρ affect the tensile behavior.

Firstly, one specimen with ρ of 0.8, η of 2 and θ of $-10°$ is selected to study the typical tensile response of nacre-like composites. Fig. 2(a) shows the experimental and simulated stress–strain curves where three feature points are marked, and the

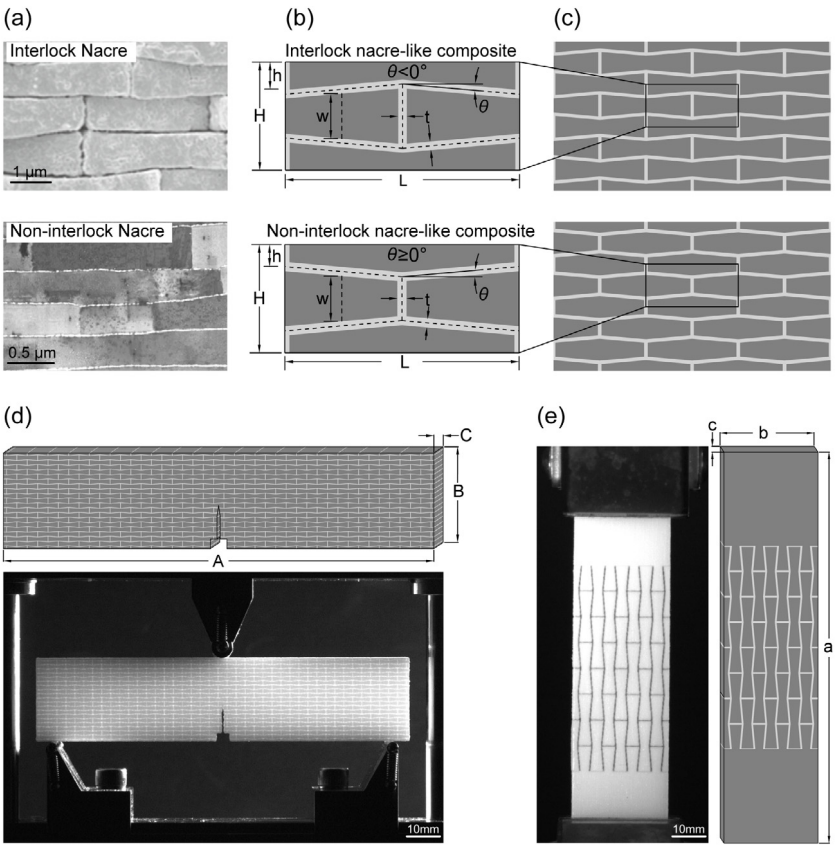

Fig. 1. Geometric design of the nacre-like composites. (a) SEM image of *Hyriopsis cumingii* with interlocked tablet [34], TEM image of *Pinctada margaritifera* with a non-interlocked tablet [35]. (b–c) Interlocking and non-interlocking nacre-like composites and unit cells. (d) SENB specimen and experiment setup. (e) Specimen for tension.

corresponding deformation and stress distribution are shown in Fig. 2(g). Point A is the first peak on the stress–strain curve, and it stands for the damage initiation on the tip interfaces marked with red lines in Fig. 2(b). Multi-layers of tip interfaces fail sequentially after point A until stress reaches the last peak of the stress–strain curve, point B. Slant interfaces damages, marked with blue lines in Fig. 2(b), happen in the structure at point B. Point C is the end of the stress–strain curve and at that point, the specimen breaks into two parts. According to the failure pattern, the stress–strain curve can be divided into 2 stages as shown in Fig. 2(c). In stage I, the first peak stands for the strength of tip interfaces which is defined as Stage-I strength, σ_{I}. In stage II, the last peak stands for the strength of slant interfaces which is defined as Stage-II strength, σ_{II}.

To study how the waviness angle θ affect the tensile performance, three specimens with fixed ρ of 0.8, fixed η of 2 and θ of $-10°$, 0°, and 10° respectively are subjected to uniaxial tension. Fig. 2(d) compares the stress–strain curves of samples with different waviness angles ($-10°$, 0°, 10°), and the corresponding deformation and failure of these specimens at the points A–C presented in Fig. 2(g)–(i). All three specimens follow the same failure pattern: one layer of tip interfaces fail first, then multilayers of tip interfaces fail, and slant interfaces fail last, which confirms the 2-stages tensile response. Stiffness and strength of the three specimens are shown in Fig. 2(e) and (f) respectively. The results show that interlocking specimen with $\theta = -10°$ has a larger stiffness and Stage-I strength than non-interlocking specimens with $\theta = 0°$ and 10°. The enhancement of stiffness and Stage-I strength in interlocking specimens is due to the increasing length of the tip interfaces and the tablets interlocking. Interlocking specimens have longer tip interfaces than non-interlocking specimens which contribute to the enhancement of Stage-I strength. More importantly, the negative waviness angle of the tablets generates interlock when tablets glide on each other. The interlock transfers more load from the tip interfaces to the tablets and inhibits the deformation and failure of tip interfaces. Such an interlocking effect can be confirmed by the stress distribution shown in Fig. 2(g)–(i), where high-stress concentration is found around the interlocked area in interlocking specimen with negative waviness angle. The results also show that the Stage-II strength of interlocking specimen is slightly larger than that of non-interlocking specimens.

To systematically study the geometrical effect of the nacre-like composites on their tensile behavior, we adjust the tablet waviness angle θ, tablet aspect ratio η and volume fraction ρ to optimize the mechanical property. One group of specimens are designed with fixed volume fraction $\rho = 0.8$, tunable aspect ratios η of 2, 5, and 10 and transitional waviness angles θ from $-30°$ to 30°. Another group of specimens is designed with fixed aspect ratio, $\eta = 5$, tunable waviness angles θ of $-10°$, 0°, and 10° and transitional volume fractions η from 0.5 to 0.9.

Fig. 3 depicts the effect of waviness angle on the stiffness and the strength of nacre-like composites. Experimental results indicate a clear trend that stiffness and Stage-I strength increase as the waviness angle decreases. Compared to specimens with waviness angles $\theta = 0°$, the stiffness and Stage-I strength of interlocking specimens increase by up to 55% and 143% respectively. However, the specimen with waviness angle $\theta = -10°$ when $\eta = 10$ does not follow the same trend. With a high aspect ratio and small waviness angle, the failure mode of this specimen does not follow the 2-Stages failure pattern. Instead, too much load is transferred into the tablets and hence the tablets break

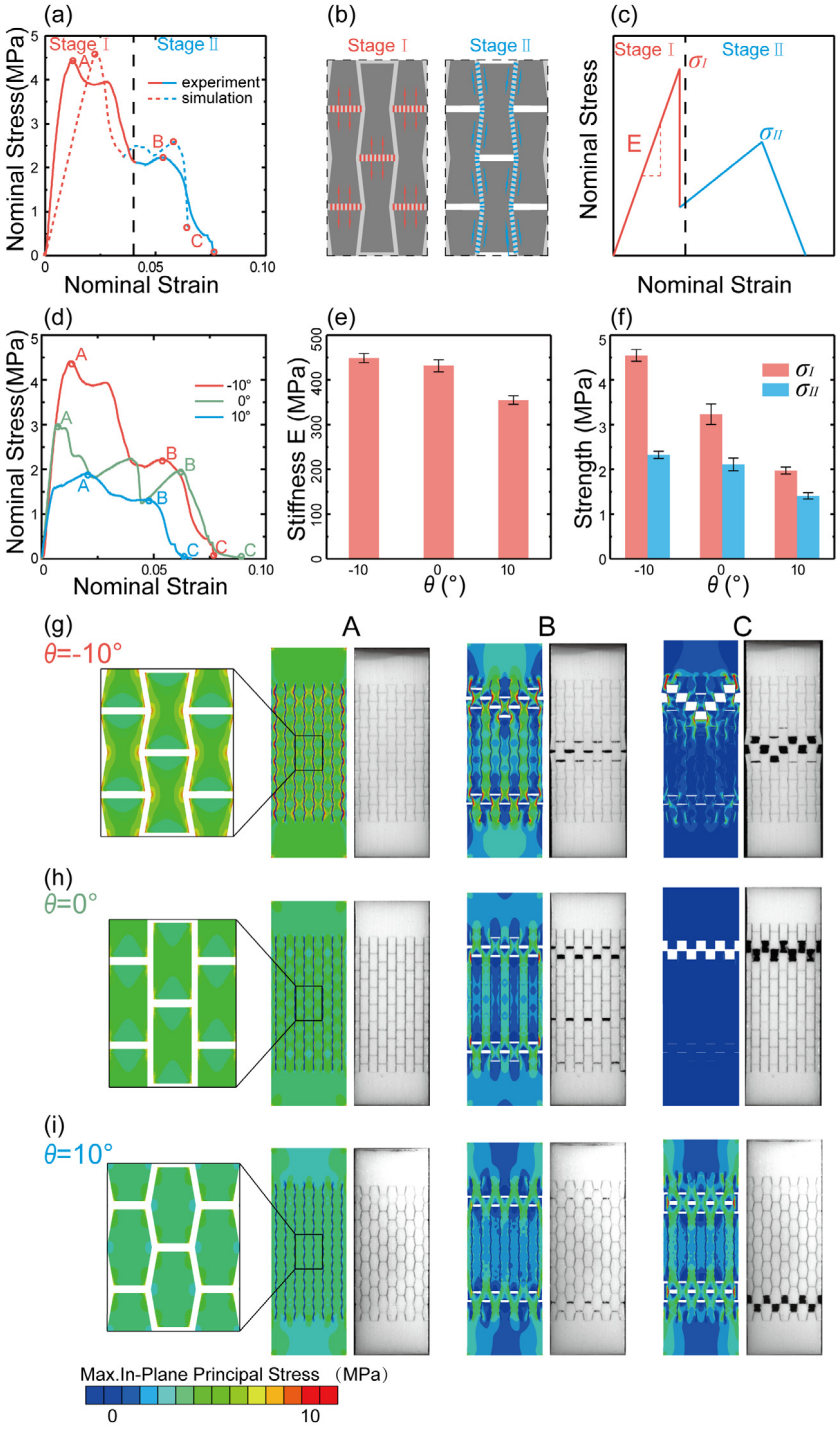

Fig. 2. Tensile behavior of three specimens with $\rho = 0.8$, $\eta = 2$ and $\theta = -10°$, 0°, and 10°. (a) Experimental and simulated stress–strain curves of the specimen with $\theta = -10°$. (b) Schematic of failure patterns in Stage I and Stage II. (c) Schematic of 2-Stages stress–strain curve. (d–f) Comparison of experimental stress–strain curves, stiffness, and strength of specimens with different θ. (g–i) Comparison of the failure pattern between simulation and experimental results of point A–C marked in (d). . (For interpretation of the references to color in this figure legend, the reader is referred to the web version of this article.)

before the failure of interfaces. The change of failure mode not only influences the tensile behavior but dramatically affects the fracture behavior, which will be discussed in the following sections. The overall strength of nacre-like composites is governed by the larger one between Stage-II and Stage-I strength. With the increase of aspect ratio η, Stage-II strength gets close to Stage-I strength and eventually becomes greater than Stage-I strength. This results in the overall strength to be governed by Stage-II strength. Moreover, Stage-II strength remains nearly constant for the specimens with the same tablet aspect ratio especially when the tablet aspect ratio $\eta = 10$. Thus, for specimens with large aspect ratio, interlocking design rarely enhances the overall strength of nacre-like composites.

Fig. 4 shows the tensile test results of the second group. The experimental results clearly show that the stiffness, Stage-I strength, and Stage-II strength all increase as the volume fraction increases for all three specimens with different waviness angles.

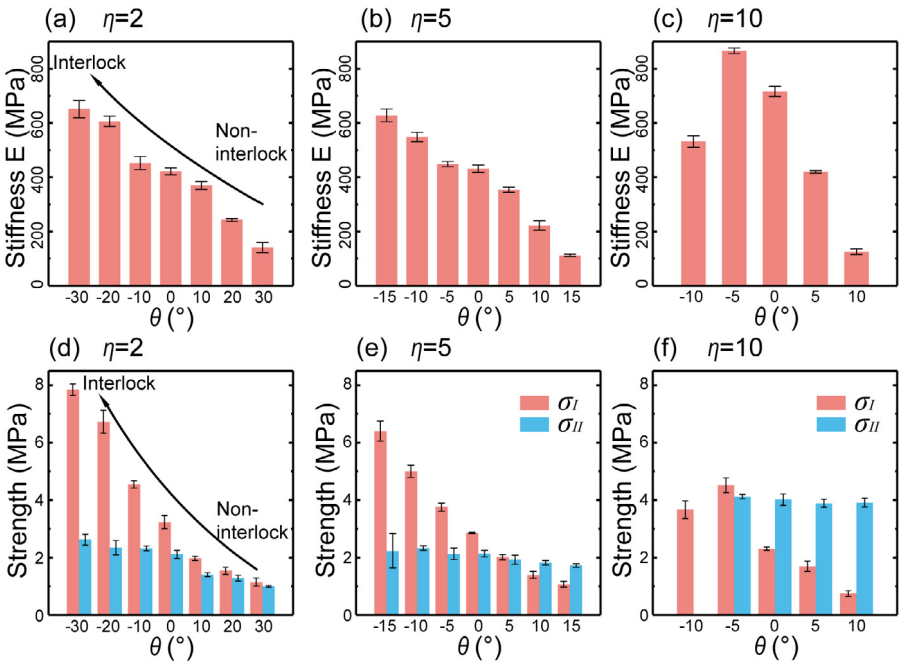

Fig. 3. Effect of tablet waviness angle on the stiffness and strength of nacre-like composites with different aspect ratios. (a–c) Stiffness. (d–f) Stage-I (red bars) and Stage-II strength (blue bars). . (For interpretation of the references to color in this figure legend, the reader is referred to the web version of this article.)

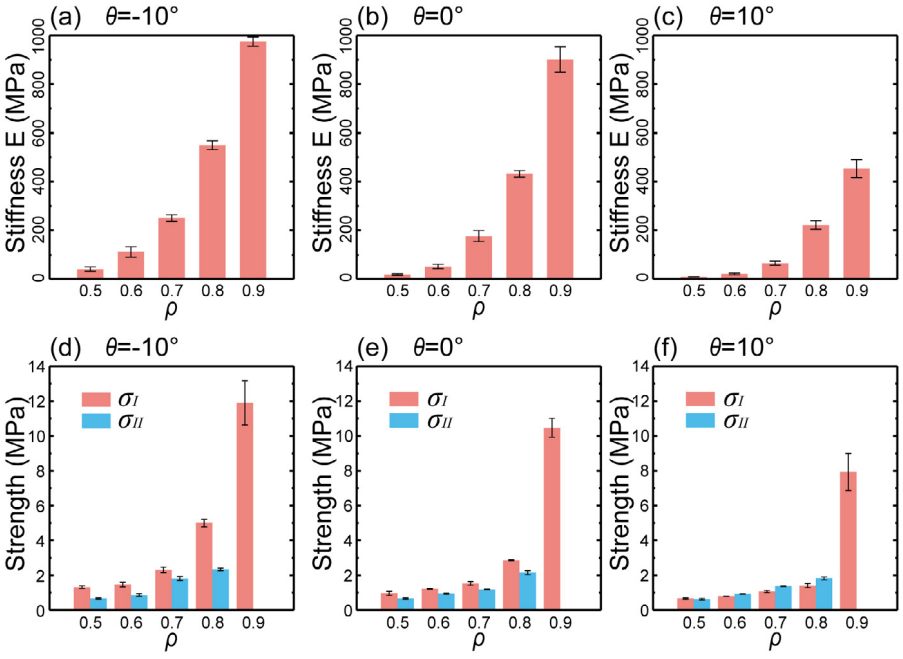

Fig. 4. Effect of volume fraction on the stiffness and strength of nacre-like composites with different waviness angles (a–c) Stiffness. (d–f) Stage-I strength (red bars) and Stage-II strength (blue bars). . (For interpretation of the references to color in this figure legend, the reader is referred to the web version of this article.)

More importantly, the enhancement of stiffness and strength exists in the interlocking design of different volume fractions.

3.2. Fracture behavior

As noted in the previous section, by choosing proper parameters, we can design nacre-like structures with both high stiffness and strength. However, strength and toughness are generally mutually exclusive. To design strong and tough nacre-like structures, we need to know how the three parameters affect the fracture behavior.

To study how the waviness angle θ affects the fracture performance, three 3D printed SENB specimens with fixed ρ of 0.8, fixed η of 5 and θ of $-15°$, $-5°$, and $15°$ are subjected to three-point bending. Fig. 5(a) compares the load–displacement curves of the three samples under 3-point bending tests. For comparison purposes, load–displacement curves of 2 SENB specimens made of base materials (Vero-White and Tango-Plus) are also shown. The load–displacement curve of the specimen with $\theta = -15°$ shows four sudden drops after reaching the peak load. The shape of load–displacement curves of specimen with $\theta = -5°$ and $15°$ are very similar — both curves start to soften after reaching the

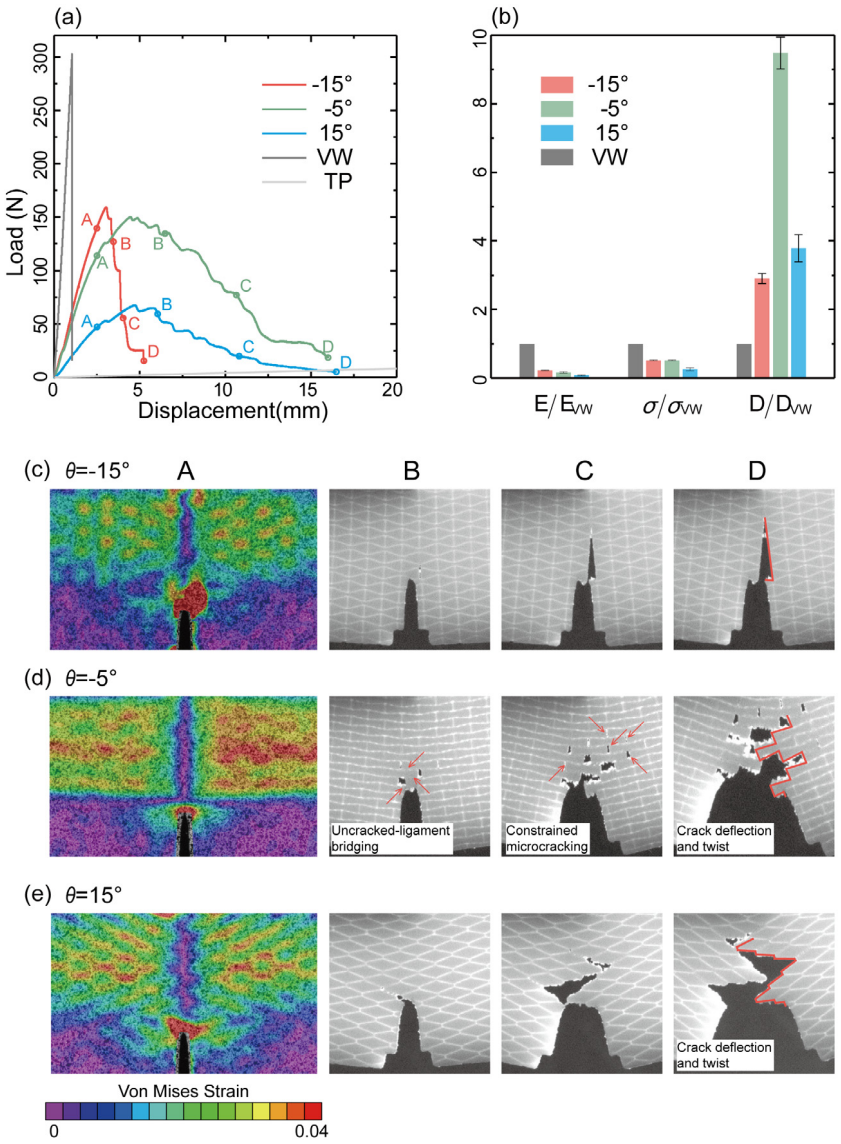

Fig. 5. Experimental results showing the effect of waviness angle on the bending behavior of SENB specimens. (a) Load–displacement curve of specimens made of base materials (TangoPlus and VeroWhite), and specimens with waviness angle $\theta = -15°$, $-5°$, $15°$, aspect ratio $\eta = 5$, and volume fraction $\rho = 0.8$. (b) Stiffness (E), strength(σ), and toughness (D) normalized by the corresponding values of the base material VeroWhite. (c–e) Strain distribution, deformation and toughening mechanisms in four continuous stages: elastic stage, crack initiation stage, crack propagation stage and fracture stage which are marked with A, B, C, and D in (a).

peak load, but at slow rates compared to the sudden drop of specimen with $\theta = -15°$.

In Fig. 5(b), the stiffness, strength, and toughness ratios between nacre-like specimens and specimen made of pure VeroWhite are shown. It follows the trends discussed in the previous section: stiffness and strength decrease as the waviness angle increases. As for the toughness, all three specimens have higher toughness than the toughness of specimen made of pure VeroWhite ($D_{VW} = 149.9$ N mm). However, the toughness of specimen with $\theta = -5°$ is much larger than those of the other 2 specimens. First, from Fig. 5(c) and (d), 2 distinct failure modes can be observed: interface failure and tablet break. The crack in specimen with $\theta = -15°$ goes directly upward and breaks through the middle of the tablets. Four tablets break during the loading which explains the four sudden drops in the load–displacement curve. While the crack in specimens with $\theta = -5°$ propagates through the interface, and the tablets are kept intact. With crack deflection and twist and tablets pulling out, interlocking specimen with $\theta = -5°$ dissipate more energy than interlocking specimen with $\theta = -15°$. With smaller waviness angle, interlocking transfers more load to the tablets that have narrower cross sections in the middle, which leads to a catastrophic tablet break due to stress concentration. Comparison of strain distribution between the two specimens can clearly confirm the higher stress concentration in specimen with smaller waviness angle. Second, if we compare Fig. 5(d) and (e), the failure modes of specimens with $\theta = -5°$ and $15°$ are the same. However, multiple toughening mechanisms are found in the interlocking specimen with $\theta = -5°$, rather than in the non-interlocking specimens with $\theta = 15°$. In the crack initiation stage (point B), comparing the deformation of the two specimens, multiple uncracked-ligament bridges are found in specimen with $\theta = -5°$ whereas no uncracked-ligament bridge is found in specimen with $\theta = 15°$. In the crack propagation stage (point C), we can find multiple constrained microcracks in the specimen with $\theta = -5°$. However, there is no constrained microcrack found in specimen with $\theta = 15°$. Crack deflection and twist are found in both specimens. All three toughening mechanisms found in specimen with $\theta = -5°$ contribute to dissipating energy during the crack propagation and increasing the toughness. Observed in

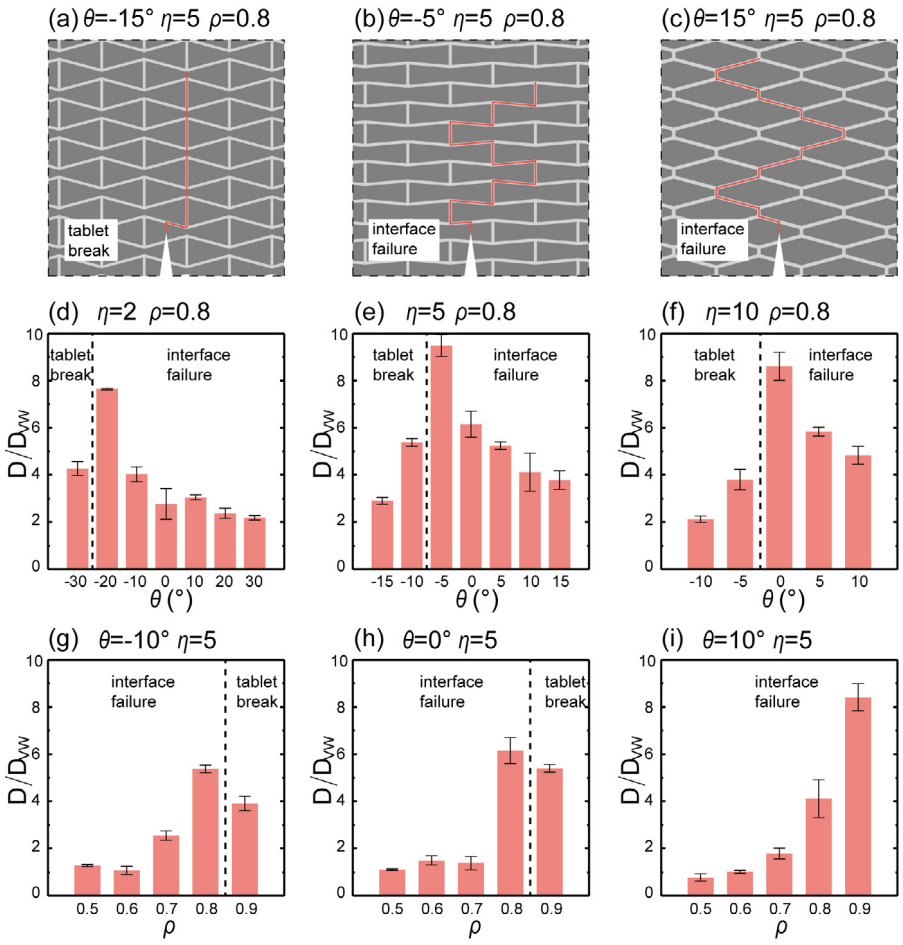

Fig. 6. (a–c) Schematics illustrating the two failure modes: interface failure and tablet break. (d–f) Normalized toughness of specimens designed with fixed volume fraction $\rho = 0.8$, tunable aspect ratios η of 2, 5 and 10 and varying waviness angles θ from $-30°$ to 30°. (g–i) Normalized toughness of specimens designed with fixed aspect ratio, $\eta = 5$, tunable waviness angles θ of $-10°$, 0° and 10° and varying volume fractions ρ from 0.5 to 0.9.

the strain contours, the interlocking in specimen with $\theta = -5°$ can transfer more load to a wider range of areas, which highly delocalizes the stress concentration and leads to the formation of uncracked-ligament bridges and multiple constrained microcracks. Furthermore, the topology of the interlocked tablets forces the crack to deflect in larger defection angle, which causes higher energy dissipation and subsequently higher toughness. Similar toughening mechanisms have been found in bone that is also built from stiff phase materials (mineral crystals) and soft phase materials (collagen molecules) [37].

To systematically study the geometrical effect of the nacre-like composites on their fracture behavior, two groups of SENB specimens are fabricated and tested. The parameters of these two groups of specimens are the same as in the previous section. Fig. 6(a–c) show the schematics of two distinct failure modes, interface failure and tablet break, observed in the experiments (Fig. 5). Experimental results indicate a clear trend that for specimens with interface failure modes, toughness increases as the waviness angle decreases. For specimens with tablet break modes, toughness decreases as the waviness angle decreases. Therefore, there is an optimized waviness angle at which the toughness researches an optimal value. The dashed lines in Fig. 6(d–f) indicates the waviness angle where two failure modes meet. Specimens in each group near this line have maximum toughness due to the competition of 2 failure modes. Therefore, when the aspect ratio and volume fraction are determined for specimens, a proper choice of waviness angle can maximize the toughness of the material. It is also seen that when the aspect ratio increases, the optimal waviness angle decreases. As shown in Fig. 6(g–i), when the aspect ratio is fixed, higher volume fraction of tablets indicates higher toughness, which is as expected. However, this is affected by the waviness angle clearly shown in the experiments. When the waviness angle is small ($\theta = 0°, 10°$), the specimen has the highest volume fraction may not have the highest toughness (Fig. 6(g) and (h)). Therefore, to find specimens with the highest toughness, it is necessary to find the optimized values of all three parameters. These will make both interface failure and tablet break maximumly contribute to the energy dissipation, indicating more materials contributes to the energy dissipation as well. Note that it is possible to build a design criterion, considering both the selection of volume ratio, aspect ratio, waviness angle and the mechanical properties of the stiff and soft phases, to predict the intersection point of the two failure modes and find the optimal parameters [38]. However, in current work, due to the nature of complex loading condition (compression and shear) and the experimental focuses, model development is not discussed and will be included in future research.

4. Conclusion

In this study, we present interlocking nacre-like composites by introducing a new parameter, tablet waviness angle, into the 'brick-and-mortar' structure usually defined with two parameters — tablet aspect ratio and volume fraction of stiff phase. Compared to nacre-like composites with flat tablet, the stiffness, strength,

and toughness of interlocking nacre-like composite increase by up to 55%, 143%, and 176% respectively. For specimens with small aspect ratio, interlocking design can improve the stiffness and strength dramatically, shown in the 2-stage stress–strain curve from tensile tests and FE simulation results. As the aspect ratio increases, the enhancement of strength due to interlocking design decreases gradually. Two failure modes are observed in the SENB fracture tests of nacre-like composites: soft phase failure and tablet break. Specimens with the highest toughness in each group are all due to the contribution of these two failure modes. Three toughening mechanisms, uncracked-ligament bridging, constrained microcracking, and crack deflection and twist, are found in interlocking specimens with highest toughness. In this study, we conclude that the toughness is not determined by one single parameter but the combination of three parameters. The key to high toughness is to choose proper combination of these parameters to transfer load to wider range of areas without causing tablet break and catastrophic failure. Note that the 3D-printed soft phase in this work exhibit rubber-like deformation behavior, which is not as complex as biopolymers. However, nacre's biopolymers have shown remarkable characteristic — deformation strengthening behavior, which plays a critical role in the strengthening and toughening of nacre [39,40], providing further design space.

Declaration of competing interest

The authors declare that they have no known competing financial interests or personal relationships that could have appeared to influence the work reported in this paper.

Acknowledgments

This research was partly supported by the National Science Foundation, USA (CMMI-1462270). The authors acknowledge the use of the Center for Functional Nanomaterials facility at Brookhaven National Laboratory.

References

[1] B. Dean, B. Bhushan, Shark-skin surfaces for fluid-drag reduction in turbulent flow: a review, Phil. Trans. R. Soc. A 368 (1929) (2010) 4775–4806.
[2] H. Gao, X. Wang, H. Yao, S. Gorb, E. Arzt, Mechanics of hierarchical adhesion structures of geckos, Mech. Mater. 37 (2–3) (2005) 275–285.
[3] A. Jackson, J.F. Vincent, R. Turner, The mechanical design of nacre, Proc. R. Soc. Lond. Ser. B 234 (1277) (1988) 415–440.
[4] S. Weiner, H.D. Wagner, The material bone: structure-mechanical function relations, Annu. Rev. Mater. Sci. 28 (1) (1998) 271–298.
[5] B. Ji, H. Gao, Mechanical properties of nanostructure of biological materials, J. Mech. Phys. Solids 52 (9) (2004) 1963–1990.
[6] F. Song, X. Zhang, Y. Bai, Microstructure and characteristics in the organic matrix layers of nacre, J. Mater. Res. 17 (7) (2002) 1567–1570.
[7] R. Wang, Z. Suo, A. Evans, N. Yao, I. Aksay, Deformation mechanisms in nacre, J. Mater. Res. 16 (9) (2001) 2485–2493.
[8] Z. Huang, X. Li, Origin of flaw-tolerance in nacre, Sci. Rep. 3 (2013) 1693.
[9] H. Li, Y. Yue, X. Han, X. Li, Plastic deformation enabled energy dissipation in a bionanowire structured armor, Nano Lett. 14 (5) (2014) 2578–2583.
[10] X. Li, W.-C. Chang, Y.J. Chao, R. Wang, M. Chang, Nanoscale structural and mechanical characterization of a natural nanocomposite material: the shell of red abalone, Nano Lett. 4 (4) (2004) 613–617.
[11] F. Barthelat, H. Tang, P. Zavattieri, C.-M. Li, H. Espinosa, On the mechanics of mother-of-pearl: a key feature in the material hierarchical structure, J. Mech. Phys. Solids 55 (2) (2007) 306–337.
[12] K.S. Katti, D.R. Katti, S.M. Pradhan, A. Bhosle, Platelet interlocks are the key to toughness and strength in nacre, J. Mater. Res. 20 (5) (2005) 1097–1100.
[13] B.L. Smith, T.E. Schäffer, M. Viani, J.B. Thompson, N.A. Frederick, J. Kindt, A. Belcher, G.D. Stucky, D.E. Morse, P.K. Hansma, Molecular mechanistic origin of the toughness of natural adhesives, fibres and composites, Nature 399 (6738) (1999) 761.
[14] Q. Cheng, M. Wu, M. Li, L. Jiang, Z. Tang, Ultratough artificial nacre based on conjugated cross-linked graphene oxide, Angew. Chem. 125 (13) (2013) 3838–3843.
[15] Z. Tang, N.A. Kotov, S. Magonov, B. Ozturk, Nanostructured artificial nacre, Nat. Mater. 2 (6) (2003) 413.
[16] S.M.M. Valashani, F. Barthelat, A laser-engraved glass duplicating the structure, mechanics and performance of natural nacre, Bioinspiration Biomimetics 10 (2) (2015) 026005.
[17] R. Libanori, D. Carnelli, N. Rothfuchs, M. Binelli, M. Zanini, L. Nicoleau, B. Feichtenschlager, G. Albrecht, A.R. Studart, Composites reinforced via mechanical interlocking of surface-roughened microplatelets within ductile and brittle matrices, Bioinspiration Biomimetics 11 (3) (2016) 036004.
[18] H. Zhao, Y. Yue, L. Guo, J. Wu, Y. Zhang, X. Li, S. Mao, X. Han, Cloning nacre's 3D interlocking skeleton in engineering composites to achieve exceptional mechanical properties, Adv. Mater. 28 (25) (2016) 5099–5105.
[19] X. Li, Z. Huang, Unveiling the formation mechanism of pseudo-single-crystal aragonite platelets in nacre, Phys. Rev. Lett. 102 (7) (2009) 075502.
[20] X. Wang, M. Jiang, Z. Zhou, J. Gou, D. Hui, 3D printing of polymer matrix composites: A review and prospective, Composites B 110 (2017) 442–458.
[21] C. Gao, B.P. Hasseldine, L. Li, J.C. Weaver, Y. Li, Amplifying. strength, toughness, Amplifying strength toughness and auxeticity via wavy sutural tessellation in plant seedcoats, Adv. Mater. 30 (36) (2018) 1800579.
[22] Z. Jia, L. Wang, 3D printing of biomimetic composites with improved fracture toughness, Acta Mater. 173 (2019) 61–73.
[23] Z. Jia, Y. Yu, L. Wang, Learning from nature: Use material architecture to break the performance tradeoffs, Mater. Des. 168 (2019) 107650.
[24] T. Li, Y. Chen, L. Wang, Enhanced fracture toughness in architected interpenetrating phase composites by 3D printing, Compos. Sci. Technol. 167 (2018) 251–259.
[25] F. Libonati, G.X. Gu, Z. Qin, L. Vergani, M.J. Buehler, Bone-inspired materials by design: Toughness amplification observed using 3D printing and testing, Adv. Energy Mater. 18 (8) (2016) 1354–1363.
[26] E. Lin, Y. Li, C. Ortiz, M.C. Boyce, 3D printed bio-inspired prototypes and analytical models for structured suture interfaces with geometrically-tuned deformation and failure behavior, J. Mech. Phys. Solids 73 (2014) 166–182.
[27] L. Liu, Y. Li, Failure mechanism transition of 3D-printed biomimetic sutures, Eng. Fract. Mech. 199 (2018) 372–379.
[28] V. Slesarenko, N. Kazarinov, S. Rudykh, Distinct failure modes in bio-inspired 3D-printed staggered composites under non-aligned loadings, Smart Mater. Struct. 26 (3) (2017) 035053.
[29] S. Askarinejad, H.A. Choshali, C. Flavin, N. Rahbar, Effects of tablet waviness on the mechanical response of architected multilayered materials: Modeling and experiment, Compos. Struct. 195 (2018) 118–125.
[30] L. Djumas, A. Molotnikov, G.P. Simon, Y. Estrin, Enhanced mechanical performance of bio-inspired hybrid structures utilising topological interlocking geometry, Sci. Rep. 6 (2016) 26706.
[31] E. Flores-Johnson, L. Shen, I. Guiamatsia, G.D. Nguyen, Numerical investigation of the impact behaviour of bioinspired nacre-like aluminium composite plates, Compos. Sci. Technol. 96 (2014) 13–22.
[32] C. Knipprath, I.P. Bond, R.S. Trask, Biologically inspired crack delocalization in a high strain-rate environment, J. R. Soc. Interface 9 (69) (2011) 665–676.
[33] P. Tran, T.D. Ngo, P. Mendis, Bio-inspired composite structures subjected to underwater impulsive loading, Comput. Mater. Sci. 82 (2014) 134–139.
[34] J. Song, C. Fan, H. Ma, L. Liang, Y. Wei, Crack deflection occurs by constrained microcracking in nacre, Acta Mech. Sinica 34 (1) (2018) 143–150.
[35] A.G. Checa, J.H. Cartwright, M.-G. Willinger, Mineral bridges in nacre, J. Struct. Biol. 176 (3) (2011) 330–339.
[36] G. Mayer, Rigid biological systems as models for synthetic composites, Science 310 (2005) 1144–1147.
[37] R.O. Ritchie, M.J. Buehler, P. Hansma, Plasticity and toughness in bone, Phys. Today 62 (2009) 41–47.
[38] Y. Liu, Z. Xu, Multimodal and self-healable interfaces enable strong and tough graphene-derived materials, J. Mech. Phys. Solids 70 (2014) 30–41.
[39] Z.H. Xu, Y. Yang, Z. Huang, X. Li, Elastic modulus of biopolymer matrix in nacre measured using coupled atomic force microscopy bending and inverse finite element techniques, Mater. Sci. Eng.: C 31 (2011) 1852–1856.
[40] Z.H. Xu, X. Li, Deformation strengthening of the biopolymer matrix of nacre, Adv. Funct. Mater. 21 (2011) 3883–3888.